
Article:
Veldman, J.K., van Kesteren, Z., Gunwhy, E.R. orcid.org/0000-0002-5608-9812 et al. (6 more authors) (2023) Accuracy of abdominal organ motion estimation in radiotherapy using the right hemidiaphragm top as a surrogate during prolonged breath-holds quantified with MRI. Medical Physics, 50 (6). pp. 3299-3310. ISSN 0094-2405

https://doi.org/10.1002/mp.16403

SGRT

USE OF **SURFACE GUIDANCE** TO HELP IMPROVE THE SAFETY, EFFECTIVENESS AND EFFICIENCY OF THE *ENTIRE* **RADIATION THERAPY** WORKFLOW

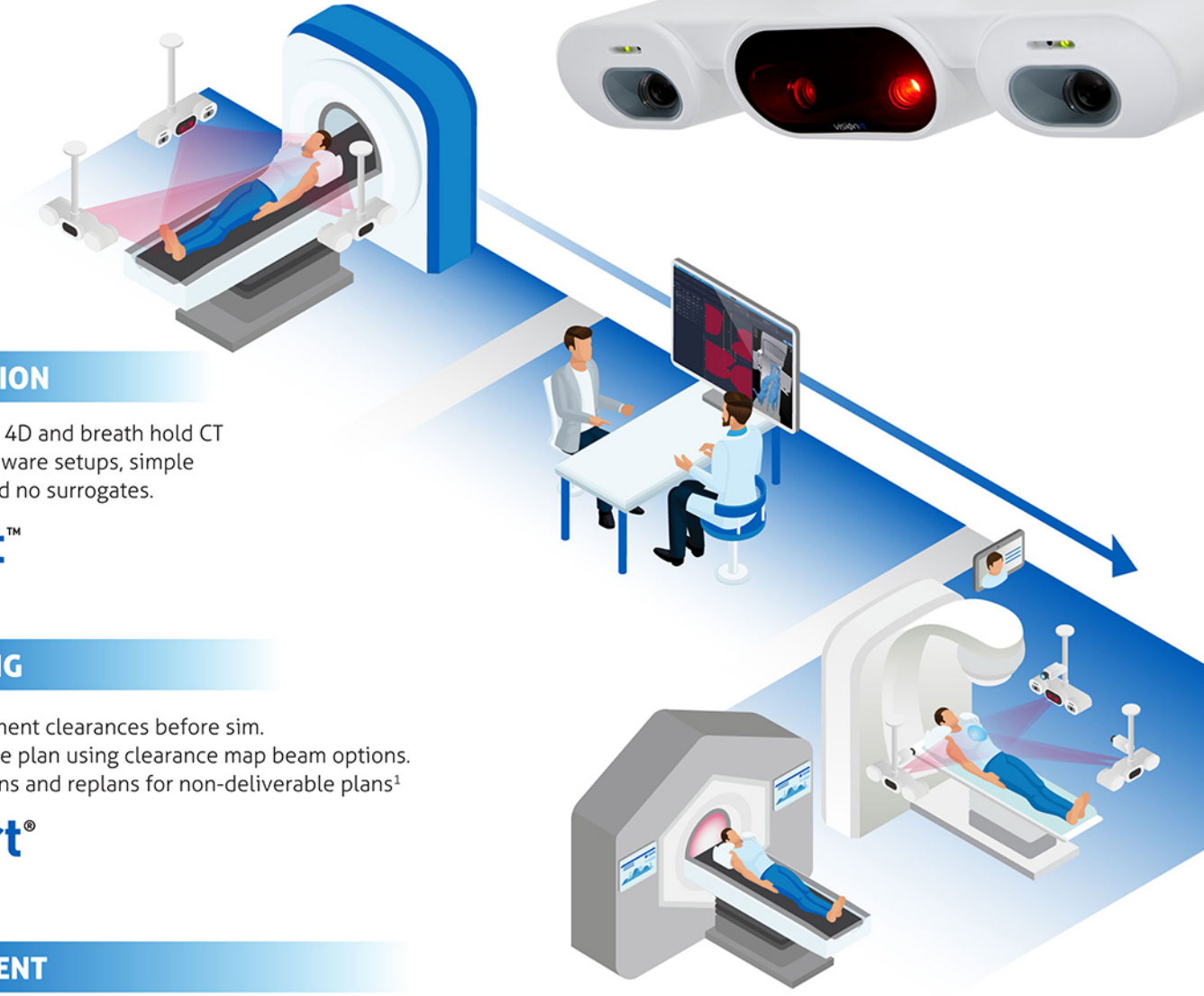

SIMULATION

Non-contact 4D and breath hold CT with no hardware setups, simple workflow and no surrogates.

simrt™

PLANNING

Check treatment clearances before sim.
Improve dose plan using clearance map beam options.
Avoid dry runs and replans for non-deliverable plans[1]

maprt®

TREATMENT

Contactless patient ID prior to treatment.
Demonstrated rapid patient setup without the need for tattoos.
TG302/ESTRO-ACROP compliant motion monitoring accuracy at all couch / gantry angle and skin tones.

alignrt® **alignrt® *InBore™***

Dose visualization can help stop treatment errors in real-time.*

dosert™
Powered by BeamSite®

1.Sheng Ke. Surface guided clearance mapping: see more, do more and achieve more. SGRT Community USA 2022

visionrt

0008-0038 - SGRT Workflow Ad v1.0

Received: 9 November 2022 | Revised: 10 February 2023 | Accepted: 20 March 2023

DOI: 10.1002/mp.16403

RESEARCH ARTICLE

MEDICAL PHYSICS

Accuracy of abdominal organ motion estimation in radiotherapy using the right hemidiaphragm top as a surrogate during prolonged breath-holds quantified with MRI

Johannes K. Veldman[1,2] | **Zdenko van Kesteren**[1,2] | **Ebony R. Gunwhy**[1,2] | **Michael J. Parkes**[1,2] | **Markus F. Stevens**[3] | **Joost G. van den Aardweg**[4] | **Geertjan van Tienhoven**[1,2] | **Arjan Bel**[1,2] | **Irma W.E.M. van Dijk**[1,2]

[1]Department of Radiation Oncology, Amsterdam UMC location University of Amsterdam, Amsterdam, The Netherlands

[2]Cancer Center Amsterdam, Treatment and Quality of Life, Amsterdam, The Netherlands

[3]Department of Anaesthesiology, Amsterdam UMC location University of Amsterdam, Amsterdam, The Netherlands

[4]Department of Pulmonology, Amsterdam UMC location University of Amsterdam, Amsterdam, The Netherlands

Correspondence
Johannes K. Veldman, Department of Radiation Oncology, Amsterdam UMC location University of Amsterdam, Amsterdam, The Netherlands.
Email: j.k.veldman@amsterdamumc.nl

Abstract

Background: Respiratory motion presents a challenge in radiotherapy of thoracic and upper abdominal tumors. Techniques to account for respiratory motion include tracking. Using magnetic resonance imaging (MRI) guided radiotherapy systems, tumors can be tracked continuously. Using conventional linear accelerators, tracking of lung tumors is possible by determining tumor motion on kilo voltage (kV) imaging. But tracking of abdominal tumors with kV imaging is hampered by limited contrast. Therefore, surrogates for the tumor are used. One of the possible surrogates is the diaphragm. However, there is no universal method for establishing the error when using a surrogate and there are particular challenges in establishing such errors during free breathing (FB). Prolonged breath-holding might address these challenges.

Purpose: The aim of this study was to quantify the error when using the right hemidiaphragm top (RHT) as surrogate for abdominal organ motion during prolonged breath-holds (PBH) for possible application in radiation treatments.

Methods: Fifteen healthy volunteers were trained to perform PBHs in two subsequent MRI sessions (PBH-MRI1 and PBH-MRI2). From each MRI acquisition, we selected seven images (dynamics) to determine organ displacement during PBH by using deformable image registration (DIR). On the first dynamic, the RHT, right and left hemidiaphragm, liver, spleen and right and left kidney were segmented. We used the deformation vector fields (DVF), generated by DIR, to determine the displacement of each organ between two dynamics in inferior-superior (IS), anterior-posterior (AP), left-right (LR) direction and we calculated the 3D vector magnitude (|d|). The displacements of the RHT, both hemidiaphragms and the abdominal organs were compared using a linear fit to determine the correlation (R^2 of the fit) and the displacement ratio (DR, slope of the fit) between displacements of the RHT and each organ. We

List of Abbreviations: 4DCT, 4-dimensional computed tomography; AP, anterior-posterior; BTFE, balanced turbo field echo; CO_2, carbon dioxide; DIBH, (short) deep-inspiration breath-hold; DIR, deformable image registration; DR, displacement ratio; DVF, deformation vector field; FB, free breathing; FOV, field-of-view; ICE, inverse consistency error; IER, inverted element ratio; IQR, inter-quartile range; IS, inferior-superior; J, jacobian determinant; kV, kilo voltage; LR, left-right; MRI, magnetic resonance imaging; O_2, Oxygen; PBH, prolonged breath-hold; RHT, right hemidiaphragm top; ROI, region-of-interest.

quantified the median difference between the DRs of PBH-MRI1 and PBH-MRI2 for each organ. Additionally, we estimated organ displacement in the second PBH by applying the DR from the first PBH to the displacement of the RHT measured during the second PBH. We compared the estimated organ displacement to the measured organ displacement during the second PBH. The difference between the two values was defined as the estimation error of using the RHT as a surrogate and assuming a constant DR over MRI sessions.

Results: The linear relationships were confirmed by the high R^2 values of the linear fit between the displacements of the RHT and the abdominal organs ($R^2 > 0.96$) in the IS and AP direction and |d|, and high to moderate correlations in the LR direction ($0.93 > R^2 > 0.64$). The median DR difference between PBH-MRI1 and PBH-MRI2 varied between 0.13 and 0.31 for all organs. The median estimation error of the RHT as a surrogate varied between 0.4 and 0.8 mm/min for all organs.

Conclusion: The RHT could serve as an accurate surrogate for abdominal organ motion during radiation treatments, for example, in tracking, provided the error of the RHT as motion surrogate is taken into account in the margins.

Trial registration: The study was registered in the Netherlands Trial Register (NL7603).

KEYWORDS
breathing control, motion surrogate, MRI

1 | INTRODUCTION

Respiratory motion presents a challenge in the treatment of thoracic and upper abdominal tumors and results in larger treatment volumes, thus increasing the risk of radiation-associated toxicities. Techniques to account for respiratory motion include tracking.[1] Magnetic resonance imaging (MRI)-guided radiotherapy systems provide tracking of tumors through direct imaging of the tumor/target.[2] Using conventional linear accelerators, tracking of lung tumors is possible directly by determining tumor motion on kilo voltage (kV) imaging.[3] But tracking of abdominal tumors with kV imaging is hampered by limited contrast. Therefore, surrogates for the tumor such as implanted fiducials,[4] external devices,[5] or internal structures[6] are used. One of the possible internal structures is the diaphragm.[7–9]

The value of the diaphragm as a universal surrogate for abdominal organs is difficult to establish during free breathing (FB),[7–9] for several reasons. First, analyzing motion of entire organs in three dimensions, requires 4-dimensional computed tomography (4DCT), that is, 3D images at, for instance, ten phases of respiration. This is prone to artefacts due to irregular breathing.[10,11] Secondly, there are substantial phase differences between diaphragm motion and motion of abdominal organs during FB.[12,13]

Breath-holding might address these issues. During all breath-holds, the diaphragm and all internal organs drift passively in predominantly the cranial direction,[14] due to the difference in gas exchange of oxygen (O_2) and carbon dioxide (CO_2) between the lungs and the bloodstream.[15] The diaphragm as surrogate during short (typically <60 s)[16] deep-inspiration breath-holds (DIBH) has been studied for pancreas tumors, with correlation of >0.8 reported for 41% of DIBHs.[14] The typically short duration of a DIBH limits the ability to accurately quantify the value of the diaphragm as surrogate.[14]

Using prolonged breath-holds (PBH) with durations of >5 min to study the diaphragm as surrogate for abdominal organ motion avoids the disadvantages of FB and the short duration of DIBH. First, the organ motion velocity is low[17] and phase differences should be negligible. Secondly, more accurate analysis is possible due to the longer duration of a PBH, during which abdominal organ displacements are larger.[17] Thirdly, the low motion velocity allows for large field-of-view (FOV) 3-dimensional MRI with minimal motion artefacts, enabling detailed analyses on motion of organs within a large FOV. For these analyses, deformation vector fields (DVF) generated by deformable image registration (DIR) have shown great potential in previous studies analyzing motion patterns.[18–21]

The aim of this study was to quantify the error when using the right hemidiaphragm top (RHT) as surrogate for abdominal organ motion during PBH for possible application during radiation treatments. We compared the displacements of abdominal organs with the gradual drift of the RHT using a linear fit. We introduced the novel term of displacement ratios (DR) between the organs of interest and the RHT to quantify this relation, and quantified the difference between DRs of repeated PBHs.

2 | METHODS

2.1 | Volunteer cohort

The study was approved by the medical ethics committee of the Amsterdam University Medical Center (NL64693.018.18). Eighteen healthy volunteers enrolled in this study, after giving written informed consent. None of them had previous experience with prolonged breath-holding. Fifteen volunteers (V1-V15; 8M/7F) with median age of 22 (range 21–62) years completed all sessions. Two volunteers dropped out during practice sessions due to communication issues and one for health reasons unrelated to the study interventions.

2.2 | Training, volunteer preparation and safety

Prolonged breath-holding, for example, breath-holding for longer than 1 min,[16] is a promising technique to control respiratory motion. This however is not widely applied in radiotherapy. This technique is feasible by non-invasive mechanical (hyper)ventilation on conscious subjects. To do this safely and comfortably, subjects are trained. Training procedures have been described previously by van Kesteren et al.[17] All volunteers were trained in two sessions to be ventilated through a facemask connected to a Hamilton MR1 mechanical ventilator (Hamilton Medical AG, Bonaduz, Switzerland). This enabled mechanical hyperventilation with 60% O_2 to reduce the end-tidal partial pressure of CO_2 to 20 mmHg inducing a state of hypocapnia, after which volunteers performed a PBH from end-inspiration for as long as they could.[22] PBH durations vary between volunteers and were at median 7 min (range 2.0-11.5 min; Table S1 in supplementary material). The PBH was terminated by the investigator if any of the safety limits was breached.[17] During a PBH, the RHT drifts passively in predominantly cranial direction by at median 3 mm/min.[17] MR images were acquired during two PBHs (PBH-MRI1 and PBH-MRI2), with at least 1 week between them. All equipment used was MRI-safe at 3T.

2.3 | MRI acquisition

During each PBH, 3D cine-MRIs were acquired on a 3T MRI (Ingenia, Philips Healthcare) using a fast balanced turbo field echo (BTFE) sequence with a FOV including the lung tops and both kidneys (Table 1). A 3D MR image was acquired every 14 s (i.e., a dynamic) resulting, in, for example, 21 dynamics over the course of a 5 min PBH. This acquisition time per dynamic should be sufficient to accurately quantify organ motion during PBH given the median 3 mm/min drift of the RHT.[17]

TABLE 1 Overview of MRI scanning parameters.

Parameter	Value
MRI strategy	3D cine-MRI
Sequence	BTFE
Resolution (mm^3)	$1.6 \times 1.6 \times 1.6$
Field of view (mm^3)	$450 \times 400 \times 240$-$280$
Echo time (ms)	1.26
Repetition time (ms)	2.5
Flip angle (°)	20
Dynamic time (s)	11.4-14.5
Slice orientation	Coronal
Water-fat shift (pixels)	0.389

Abbreviation: BTFE, balanced turbo field echo.

We then determined organ displacements by: (1) generation of DVFs using DIR on a selection of dynamics, (2) segmentation of regions-of-interest (ROI), and (3) calculation of ROI displacements using the DVFs.

2.4 | Image registration

For image registration, seven dynamics were selected (the first, dynamics at 25%, 50%, and 75% of the PBH duration, and the last three). A groupwise approach of a DIR algorithm was implemented via Elastix v.5.0 (Image Sciences Institute, University Medical Centre Utrecht, The Netherlands)[23] with all seven dynamics input as a 4D volume (i.e., a time-series of 3D MRI volumes). From this 4D volume, a virtual reference image was created as a mean of the seven dynamics. The groupwise registration consisted of forward registrations, that is, from each of the dynamics towards the virtual reference, and inverse registrations from the virtual reference to each of the dynamics (Figure 1).[24] The DIR algorithm used a 2^{nd} order B-spline transformation model and optimized a variance over last dimension metric in the forward registrations, and a displacement magnitude penalty metric in the inverse registration (configuration files in supplementary material). This groupwise approach yields a set of DVFs between each volume and a virtual reference volume. From these DVFs, registrations between each dynamic with respect to the first dynamic were calculated. This was done by summation of the DVF of the forward registration of Dyn_1 to Dyn_R and the DVF of the inverse registration of the respective dynamics to Dyn_R (Equation 1).

$$DVF\ (Dyn_1 \rightarrow Dyn_N) = DVF\,(Dyn_1 \rightarrow Dyn_R) + DVF^{-1}\,(Dyn_N \rightarrow Dyn_R) \quad (1)$$

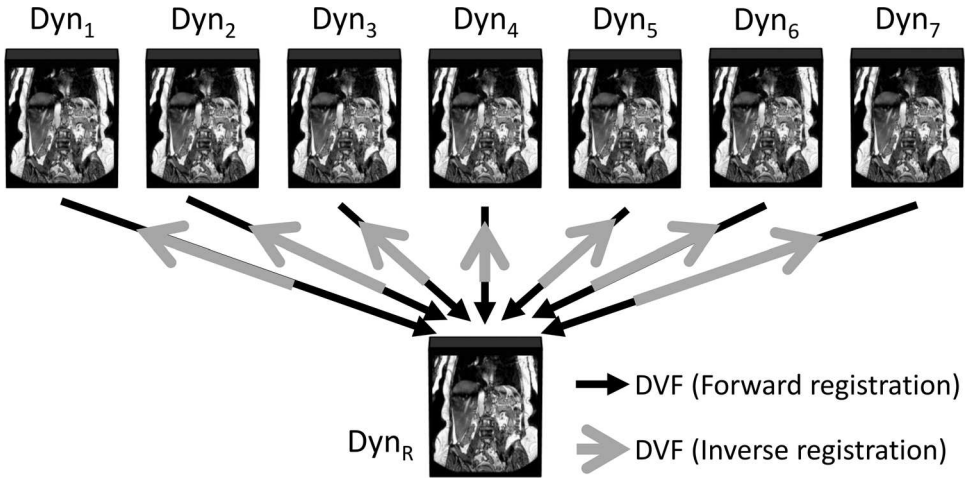

FIGURE 1 Groupwise deformable image registration. The black arrows indicate the forward registrations from the seven dynamics (Dyn_1 – Dyn_7) to the virtual reference (Dyn_R). The gray arrows indicate the inverse registrations from the virtual reference to the seven dynamics. Deformation vector fields (DVFs) from the first dynamic to any subsequent dynamic were calculated by summing the DVFs from a forward registration and an inverse registration following Equation (1).

2.5 | Quality assurance

The precision of the calculated displacements depends on the accuracy of the registration. Therefore, the registration quality was assessed using two quality metrics: the inverse consistency error (ICE)[25] and the inverted element ratio (IER).[26] The ICE provides a measure of the consistency of registrations of two dynamics and was defined as the remaining displacement after vector composition of both the forward and inverse DVFs of a registration. The IER employs the spatial Jacobian determinant J, providing a measure of the deformation that a voxel is subjected to. J is defined as the quotient of the deformed and undeformed volume, and the outcome depicts the type of deformation that has occurred, that is, local expansion ($J > 1$), local compression ($J < 1$) or no change ($J = 1$) whereas $J < 0$ indicates tissue loss. The latter indicates "foldings" in the transformation matrix, meaning that part of the voxel disappeared. As this is physically not plausible, any inverted elements in J would indicate registration failure. The IER is then defined as the quotient of the number of inverted elements and the total number of elements (Equation 2).

$$IER = \frac{\#\ of\ inverted\ elements}{Total\ \#\ of\ elements} \quad (2)$$

ICE values of <1 mm[27] and IER of <0.27%[28] were considered as acceptable values for DVF quality.

2.6 | Diaphragm and abdominal organ segmentation

Four trained observers segmented the liver, the spleen, the right and left kidney, right and left hemidiaphragm and RHT upon the first dynamic of each PBH (Figure 2). The liver, spleen and right and left kidneys were segmented using departmental delineation guidelines, and discussed to reach consensus. The hepatic veins and the left portal vein were included in the liver delineation whereas the inferior vena cava was excluded. The spleen was delineated excluding the splenic hilum. The kidney delineations included the pyelum but not the hilum. Furthermore, the superior 1 cm of the liver (i.e., the liver dome) was segmented to be used as a surrogate for the right hemidiaphragm. Any area located caudally from the heart or left lung was excluded from this segmentation. The RHT was defined as a region with a 1.5 cm radius centered on the most cranial point

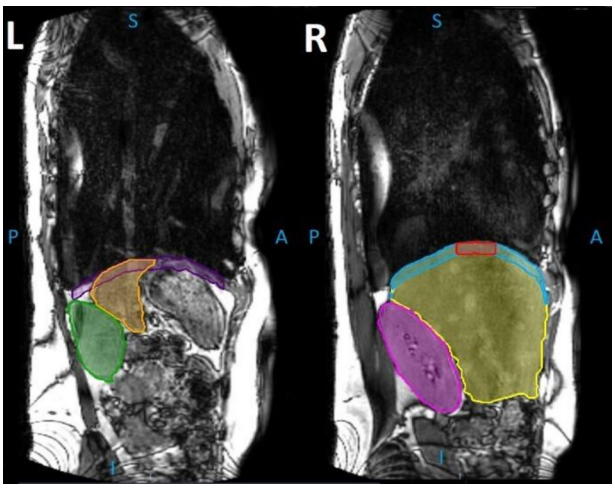

FIGURE 2 Diaphragm and abdominal organ segmentations. Segmentations of the diaphragm and abdominal organs visualized in a single sagittal slice for the left (L) and right (R) side. L: the left kidney (green), the spleen (orange) and the left hemidiaphragm (purple). R: the right kidney (pink), the liver (yellow), the right hemidiaphragm (blue) and the right hemidiaphragm top (red).

of the right hemidiaphragm and was extracted from the right hemidiaphragm segmentation. The left hemidiaphragm was segmented by delineating a 1 cm volume below the left lung-abdomen interface as surrogate for the left hemidiaphragm (Figure 2). All procedures were performed in Velocity AI software v.4.1. (Varian Medical Systems Inc.). The segmentations were exported in Radiotherapy Structure DICOM format and converted into NIFTI format using 3D Slicer software v.4.10.2 r28257[29] for subsequent motion analysis.

2.7 | Displacement quantification

Each voxel within a DVF contains the 3D displacement between two dynamics from which the inferior-superior (IS), anterior-posterior (AP), and left-right (LR) components were extracted and the 3D displacement magnitude (|d|) calculated. To determine organ displacement, the vectors encompassed by a specific organ were selected. Subsequently, the voxel count per displacement value was computed and visualized in a histogram for each organ, showing the displacement distribution. Displacement values centered on a single sharp peak indicated relatively rigid displacement, whereas a broader distribution or multiple peaks were indicative of a more heterogeneous movement pattern within the organ such as rotation and deformation. From the distributions we determined the median value as representative value of organ displacement as this value best represented motion of the entire organ. We chose the inter-quartile range (IQR) as a measure of displacement uncertainty.

2.8 | Analyses

Displacements in all directions of all organs over time were calculated separately for PBH-MRI1 and PBH-MRI2 per volunteer and were plotted against the displacement of the RHT for PBH-MRI1 and PBH-MRI2. These data points were linearly fitted, and the correlation coefficient R^2 was calculated. Since this linear fit was fixed at (0,0), R^2 values are limited from 0 at weak to 1 at strong correlation. The slope of the linear fit, that is, the DR, was calculated to quantify the relation between the displacements of the RHT and the abdominal organs. The DR is defined such that a value between 0 and 1 implies that the RHT has a larger displacement than the abdominal organ, and a value larger than 1 implies that the abdominal organ has a larger displacement than the RHT. Figure 3 shows an example how the R^2 and DR were calculated for the displacement magnitude |d| of the RHT versus the right kidney. To establish the reproducibility of the DR between PBH-MRI1 and PBH-MRI2 for individual volunteers, the absolute difference and signed difference between the DRs have been

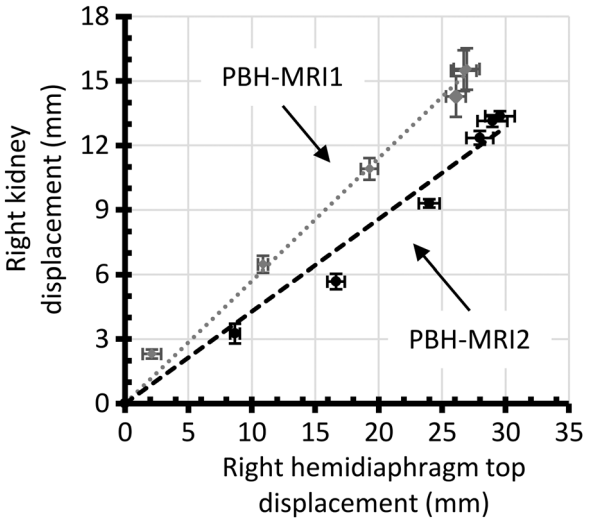

FIGURE 3 Correlation plot between the displacement of the right hemidiaphragm top and right kidney. An example of the linear fit of the displacement magnitude |d| of the right hemidiaphragm top versus displacements of the right kidney for PBH-MRI1 (gray) and PBH-MRI2 (black) of one volunteer. From the linear fit, R^2 and the displacement ratio (DR; slope of the fit) were extracted for further analysis. R^2 values in this example are 0.99 (PBH-MRI1) and 0.97 (PBH-MRI2); displacement ratios (slope of the linear regression lines) are 0.57 (PBH-MRI1) and 0.43 (PBH-MRI2). The DR difference is 0.14.

calculated. The error of the RHT as a motion surrogate for each organ was calculated using Equation (3) as the difference between estimated displacement (first term) and actual displacement (second term) during PBH-MRI2.

$$error = (DR_{PBH-MRI1} \times displacement_{RHT,PBH-MRI2}) - displacement_{organ,PBH-MRI2} \quad (3)$$

The Shapiro Wilk's test combined with Q-Q plots indicated that the data was not normally distributed. We, therefore, used Wilcoxon's signed rank test to determine significance of differences. A two-tailed p-value of <0.05 was considered statistically significant. All statistical analyses were performed using SPSS (SPSS Statistics Version 26, IBM, Armonk NY).

3 | RESULTS

Thirty MRI datasets acquired from 15 volunteers performing PBHs were eligible for analysis. Two datasets could not be analyzed due to an error in creating the 4D volume required as input for the DIR algorithm. In the remaining 28 datasets, the RHT, both hemidiaphragms, the liver and spleen were included for analysis. In one dataset, the left kidney had to be excluded due to partially being outside the FOV, leaving $n = 27$ left kidneys to be analyzed. The right kidney was excluded in four

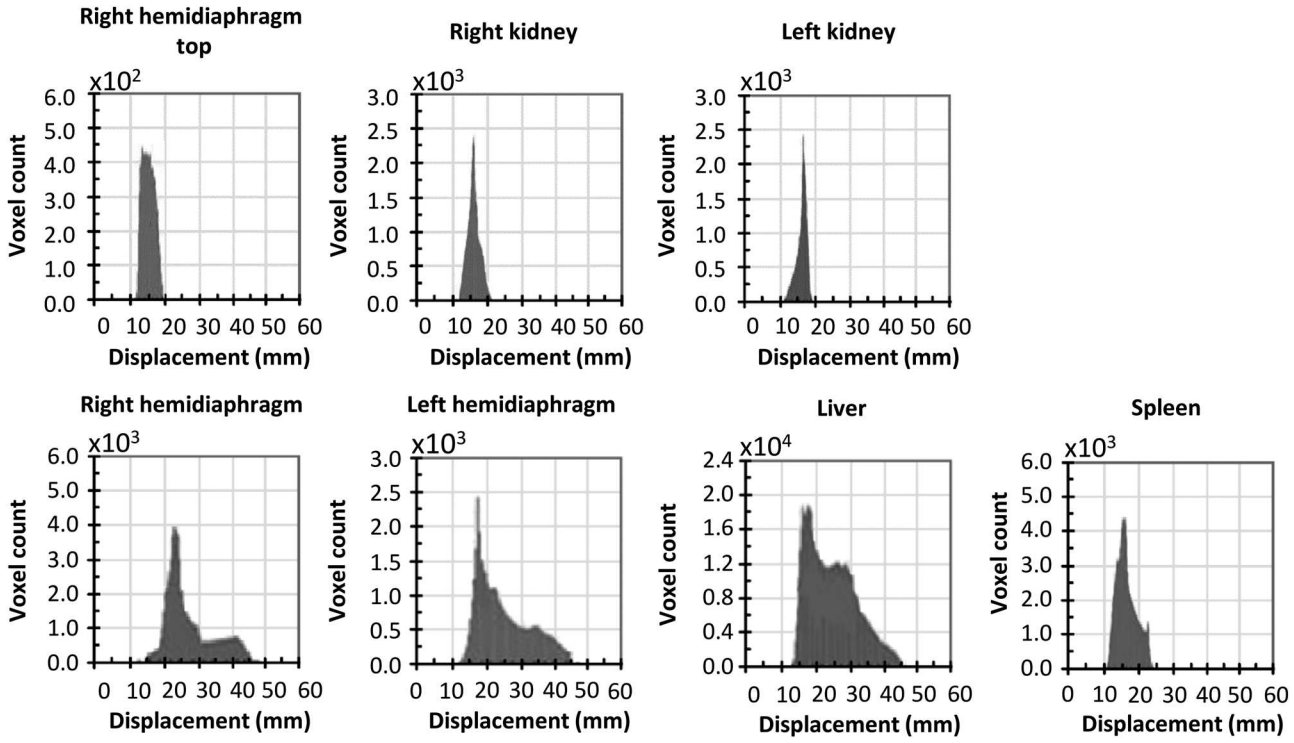

FIGURE 4 Typical displacement distributions of the displacement magnitude |d| for all investigated organs. Distributions of rigid-like displacement are characterized by a single sharp peak, whereas a distribution of deformable, less rigid displacement is characterized by a broad distribution with (possibly) multiple peaks. Displacement distributions were classified as rigid-like for the right hemidiaphragm top, right kidney and left kidney or less rigid displacement for the right hemidiaphragm, left hemidiaphragm, liver and spleen.

datasets due to partially being outside the FOV ($n = 2$) and due to a coincidental finding unrelated to the study interventions ($n = 2$), resulting in $n = 24$ right kidneys for analysis. No DVFs were excluded because all ICE values were <1 mm (median 0.006 mm, IQR 0.015 mm) and all IER values were <0.27% (median 0.00%, IQR 0.02%).

3.1 | Distributions of displacement magnitude

Typical examples of distributions of displacement magnitude |d| for the organs under investigation are shown in Figure 4. These reflect the displacement of each organ from the first to the last dynamic, selected from various PBHs. Rigid displacement of an organ would lead to a high voxel count around a single value, resulting in a displacement distribution with a single, sharp peak. Less-rigid, deformable displacement of an organ would lead to high voxel counts at different displacement values, resulting in a broad distribution and (possibly) multiple peaks. Rigid displacement distributions were found for the RHT and both kidneys whereas deformable, less rigid displacement distributions were found for both hemidiaphragms, the liver and -to a lesser extent- the spleen. To best summarize organ displacement, we extracted the median value as representative value and IQR as uncertainty measure.

3.2 | Diaphragm and organ displacement during PBH

Figure 5 is an example of the typical displacements of all organs over the course of a PBH in all directions and |d|, with a linear fit for each organ. This linear drift is observed for all organs in all PBHs. The IS displacement is the dominant component in |d| for the RHT, both hemidiaphragms and the liver. AP and IS displacements are equally dominant for the spleen and the AP displacement is dominant for both kidneys. Moreover, right sided-organs typically move to the left whereas left-sided organs move to the right.

3.3 | Correlation between displacements of abdominal organs and the RHT

Since the RHT, both hemidiaphragms and all abdominal organs displace with a linear drift, we expect a high correlation between the RHT and abdominal organs. We analyzed R^2 values of the linear fit between

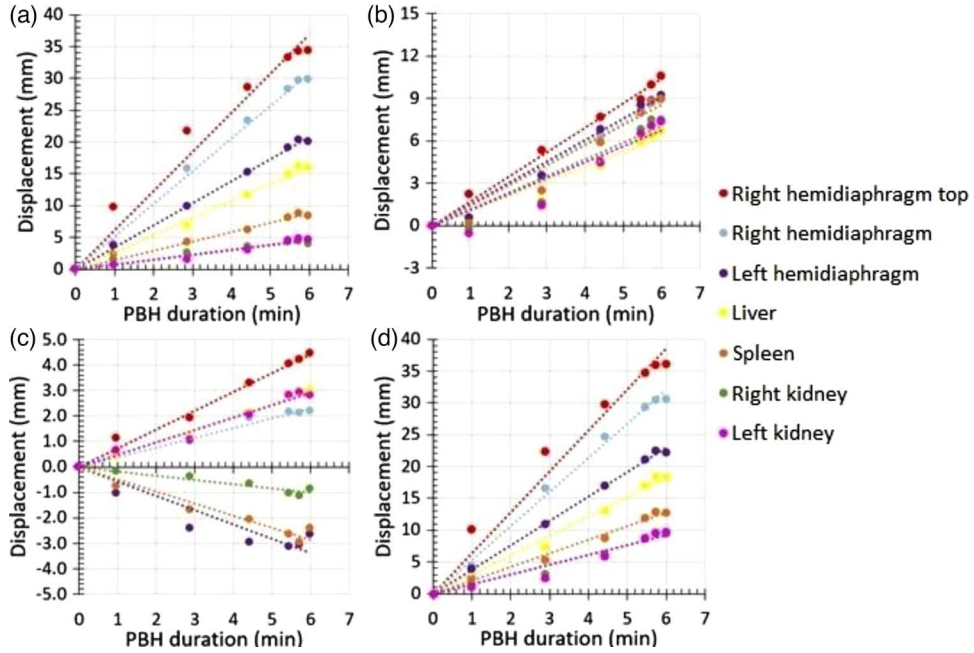

FIGURE 5 Linear drift over time of all organs during a single PBH. Typical examples of displacements of the right hemidiaphragm top, left and right hemidiaphragm and the abdominal organs under investigation over time during a prolonged breath-hold of one subject in three directions: (a) inferior superior direction, (b) anterior-posterior direction (c) left-right direction (d) and the displacement magnitude |d|. Positive values indicate (a) superior, (b) posterior and (c) left direction of displacement. Note that y-axis scales differ. All organs/structures show a linear drift over time in each direction.

TABLE 2 : Correlation between the displacements of the right hemidiaphragm top and both hemidiaphragms and abdominal organs.

Correlation (R^2) between RHT and	IS Median (Q3-Q1)	AP Median (Q3-Q1)	LR Median (Q3-Q1)	|d| Median (Q3-Q1)
Right hemidiaphragm	1.00 (1.00-0.99)	1.00 (1.00-0.98)	0.93 (0.98-0.52)	1.00 (1.00-0.99)
Liver	0.98 (1.00-0.97)	0.98 (0.99-0.95)	0.89 (0.97-0.53)	0.99 (1.00-0.98)
Right kidney	0.99 (0.99-0.95)	0.97 (0.99-0.89)	0.64 (0.95-0.41)	0.99 (1.00-0.97)
Left hemidiaphragm	0.99 (1.00-0.97)	0.99 (1.00-0.97)	0.77 (0.91-0.19)	0.99 (1.00-0.99)
Spleen	0.99 (1.00-0.96)	0.97 (0.99-0.90)	0.78 (0.94-0.09)	0.99 (1.00-0.98)
Left kidney	0.98 (0.99-0.96)	0.97 (0.99-0.80)	0.80 (0.93-0.59)	0.99 (1.00-0.97)

Note: R^2 values were derived from the linear fit between the displacements of the right hemidiaphragm top and both hemidiaphragms and abdominal organs. High correlations (R^2 ≥0.97) were found for all directions except left-right (0.64-0.93).
Abbreviations: |d|, 3D vector magnitude; AP, anterior-posterior; IS, inferior-superior; LR, left-right; RHT, right hemidiaphragm top.

displacements of the RHT and both hemidiaphragms and abdominal organs over all PBHs in the three cardinal directions and for the displacement magnitude |d|. Median R^2 values over all volunteers were at least 0.97 for all directions except for LR (minimum 0.64) (Table 2). Lower values of R^2 for the LR component of the displacement are expected due to the smaller displacement in LR direction, approaching the voxel resolution of the scan. For each organ individually, the variation in R^2 was least where displacement was greatest (i.e., their IQRs increased from |d| < IS < AP < LR). For the AP direction the IQR was least when nearest to the diaphragm, but this was not the case for the other directions.

If there would be no difference in DRs between PBH-MRI1 and PBH-MRI2, using the RHT as a surrogate for abdominal organ motion would be highly accurate. However, there was always a measurable, though small, difference (Figure 6). The smallest difference (0.13) was between the RHT and the right hemidiaphragm that is, every millimeter displacement of the RHT, would result in a median error of 0.13 mm when estimating the displacement of the right hemidiaphragm. For the right side, the more caudal the organ, the greater the difference (0.17 for the liver, 0.21 for the right kidney). This trend was not apparent on the left side (0.31 for the left hemidiaphragm, 0.17 for the spleen, and 0.29 for the left kidney). Signed differences were randomly

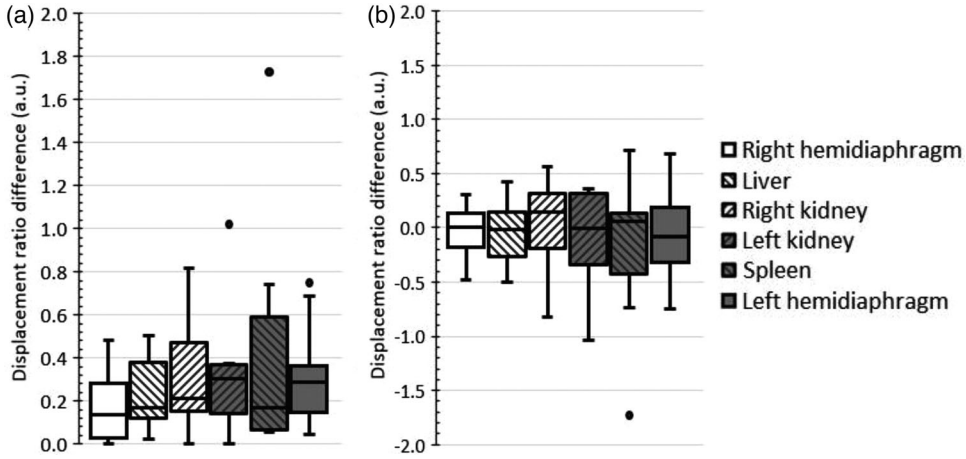

FIGURE 6 Box-plots showing displacement ratio differences between PBH-MRI1 and PBH-MRI2. (a) Absolute values of displacement ratio differences and (b) signed displacement ratio differences for the different organs. Absolute differences show large differences between prolonged breath-holds. Signed differences show that these differences are distributed around zero. Boxes: median value and lower and higher quartiles, whiskers: lowest and highest data point within 1.5 times the inter-quartile range.

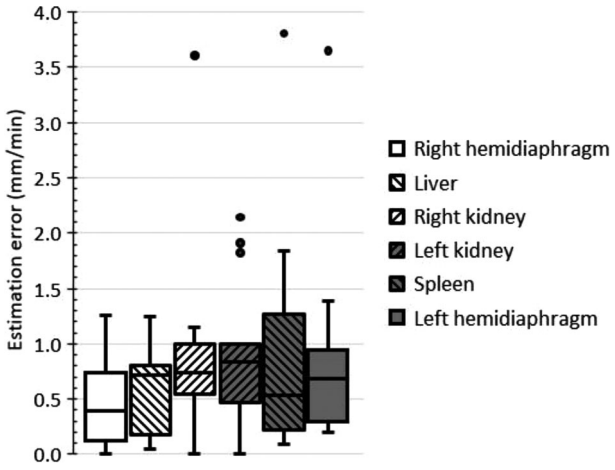

FIGURE 7 Low error in estimating abdominal organ motion using the right hemidiaphragm top. Error in mm/min of the right hemidiaphragm top estimating displacement of each organ. The median error of the right hemidiaphragm top as a surrogate for all organs varied between 0.4 and 0.8 mm/min. Boxes: median value and lower and higher quartiles, whiskers: lowest and highest data point within 1.5 times the inter-quartile range; "x" denotes the mean value.

distributed around zero and not significantly different from zero (Wilcoxon's sign rank test, $p > 0.05$). All DRs for all organs and each individual PBH can be found in the supplementary materials (Figures S1–S6).

The median error of the RHT as a surrogate for each organ varied between 0.4 and 0.8 mm/min (Figure 7). No obvious trend in error magnitude with IS or LR organ location was observed.

4 | DISCUSSION

The diaphragm and upper abdominal organs move as a result of breathing. Residual motion exists even during PBHs in the form of a gradual drift.[17] In this study, we quantified the error when using the RHT as surrogate for abdominal organ motion during PBH for possible application in radiation treatments. We demonstrated a novel method using DIR to calculate organ displacements over a large FOV, and found high R^2 values (i.e., strong correlations) between displacements of the RHT and both hemidiaphragms and abdominal organs in IS and AP directions and for the vector magnitude |d|. We also showed that abdominal organ motion can be accurately estimated when using the RHT top as surrogate during PBH, since the error is in the order of 1–3 millimeters for each centimeter of RHT displacement and below 1 mm per minute of breath-holding.

The correlation between the displacement of diaphragm and abdominal organs has been quantified previously by several techniques, mostly by assessing displacements of landmarks or tumors, which resulted in a local measure of displacement.[7–9] Siva et al. correlated probability density function of diaphragm motion with cranio-caudal motion of the kidney apex[7]. Yang et al. applied a normal-cross-correlation algorithm to quantify correlation between diaphragm motion and liver tumor motion on 2D MR images.[8] Feng et al. quantified the correlation between motion of superior and inferior pancreas tumor borders and the diaphragm also on 2D MR images.[9] We chose a more global strategy applying DIR to quantify organ displacements, which has the advantage that the calculated displacement distributions provide a more general picture of the motion including translations and deformations determined from the calculated DVFs. ICE and IER values of respectively <1 mm and <0.27% showed that the registration quality was high. Therefore, we could accurately quantify organ translations and deformations across the entire FOV.

We have chosen to summarize displacement distributions of rigid and less rigid organ displacement in a single representative value. However, this single value may not always be representative for the entire organ or structure. The liver, for example, has several lobes which to some extent can displace independently,[30–32] and diaphragm displacement is limited at the medio-ventral side, and larger at the latero-dorsal side.[33] Separating structures or organs into different segments might provide a better description of the displacement of each segment as we demonstrate for differences in displacement distributions of the right hemidiaphragm and RHT. Using heat maps or deformation models[34] might be helpful to accurately define different segments of an organ with different displacement magnitudes.

We selected the RHT as surrogate since it is a clearly distinguishable landmark on the diaphragm. Nevertheless, the RHT is not the part of the diaphragm that drives the motion during a PBH nor has it the largest displacement. Several segments of the diaphragm have different displacement magnitudes and therefore influence displacements of abdominal organs, depending on their location. The kidneys may displace more than the RHT, due to their retroperitoneal position. We observed that in the DR, which is >1 in numerous cases for both kidneys. This is much less the case for the liver, only in 3 out of 27 PBHs.

The strong correlations between displacements of the RHT and both hemidiaphragms and abdominal organs are similar to the results of Yang et al.[8] Using a normalized cross correlation tracking technique, they found strong correlations between motion of the RHT and liver tumors during FB in IS and AP directions (r = 0.97 and r = 0.98, respectively). The moderate to strong correlations (median R^2 of 0.64–0.93) in LR direction that we found are greater than what Yang et al. reported (r = 0.08)[8]. We also found greater correlations between the displacement of the ipsilateral hemidiaphragm and both kidneys in IS direction than reported by Siva et al. (r = 0.52 and r = -0.18 for the right and left kidney, respectively).[7] Our R^2 values are also greater than previously reported in literature for other abdominal organs. Feng et al. compared motion of superior and inferior pancreas tumor borders with that of the right hemidiaphragm on 4DCT images during FB and reported weak correlations between the motion of the right hemidiaphragm and that of pancreatic tumors ($-0.18 < r < 0.43$).[9] Lens et al. found high correlations ($r > 0.8$) between motion of the RHT and pancreatic tumor fiducials during DIBH on 30 s CBCT movies in 41% of DIBHs in IS direction and 22% of DIBHs in AP direction.[14]

Lens et al. used a pooled approach to measure the slopes of the correlation plots for diaphragm displacement versus displacement of fiducial markers in the pancreas during DIBH. They concluded that the diaphragm was not a reliable surrogate for pancreatic tumor motion during DIBH[14] and recommended an individual approach. Following this recommendation, we determined the DR, the slope of the linear fit, for each PBH separately, and showed that the RHT can be used to accurately estimate abdominal organ motion. Our results also show that variation in DR differences increased with more caudal organ location. This is in agreement with results of Huijskens et al., who found in paediatric cancer patients that position variation of the ipsilateral diaphragm was more representative for position variations of the liver and spleen than for kidney position variations.[35] Additionally, we observed differences in DR within volunteers, that is, between PBHs of individual volunteers. It has been previously reported that respiratory patterns may change during radiation therapy,[36] however the drift of the RHT and all organs is linear throughout the PBH with constant velocity. This drift is variable between subjects and between PBHs, as the gas exchange in the lungs depends on the metabolism of the person at that very moment. Since we cannot control this, we estimated the displacement errors of the various organs when using a measured drift of the RHT during one PBH and apply this to organ motion during subsequent PBHs. The difference in DRs between these PBHs may be partially caused by variations in initial diaphragm position of repeated inspiration breath-holds, as we reported previously.[17] However, although the initial diaphragm position at the start of repeated PBHs was equal in three volunteers, the DRs during each of these PBHs varied. These variations in DR may be caused by inter-fraction anatomical variation, such as stomach filling, which could influence displacements of nearby organs.[37,38]

A strength of our study includes the typically longer durations of PBHs (2–12 min),[17] which enabled us to accurately analyze the validity of the RHT as surrogate for displacements of both hemidiaphragms and abdominal organs, since larger displacements occur during PBH compared to DIBH. It would be interesting to generalize our results to DIBH and/or FB, since these are used in clinical practice. During DIBH, the error in estimating abdominal organ motion using RHT is expected to be in the order of sub-millimeters, since the median estimation error during PBH is <1 mm/min (Figure 7), whereas the DIBH duration is less than 60 s.[16] However, it has been shown that an initial (and larger) settlement of the diaphragm occurs during the first 10 s of DIBH.[39] Similarly, to DIBH in clinical practice, PBHs with 5 min duration may be repeated up to 9 times, by re-introducing hypocapnia within 3 min.[40] The DR difference, which provides an error based on the displacement of the RHT rather than breath-hold duration, could be used to take into account the initial settlement of the diaphragm at the start of a DIBH. Generalizing our results to FB, for example during tracking, is a bit more challenging. During breath-holding, the diaphragm

and abdominal organs drift passively due to the gas exchange between the lungs and the bloodstream.[15] Contrarily, organ displacements during FB are caused by the diaphragm actively driving respiratory motion. Although the biomechanics are different and a phase difference between diaphragm motion and abdominal organ motion exists, we may assume that the DRs found here during PBH might be roughly similar during FB. This would allow the use of the DR to estimate the magnitude of abdominal organ motion based on the motion of the RHT, with a median error of 0.13-0.31 cm for every cm of RHT displacement.

PBHs may solve several limitations in tracking as mentioned in previous studies.[3,41] Remmerts et al. investigated markerless tracking of lung tumors using kV imaging during FB and reported on the occurrence of time intervals without successful tracking of the moving tumor due to image saturation, as a result of over projection of the spine. When applying PBH instead of FB, motion during such time intervals without tracking would be minimal due to the 3 mm/min drift of the diaphragm. Consequently, the potential dosimetric consequences of unsuccessful tracking would be decreased. Similarly, Hindley et al. used kV imaging to track the diaphragm and investigate the applicability of using the diaphragm as surrogate for lung tumor motion.[41] They found that when the spine occluded the left diaphragm the algorithm would track the right diaphragm, resulting in a time interval with erroneous estimations of left lung tumor motion. The dosimetric impact of these erroneous estimations might decrease when tracking would be performed during PBH, since motion during this time interval with unsuccessful tracking would be minimal. Other sources of error reported by Remmerts et al. include a limited number of previous matches, where a small mismatch may result in a large deviation in estimated 3D position.[3] During PBH, displacements are slow and gradual, and mismatches are expected to occur less. Also, Hindley et al. use a restricted search window based on the previous diaphragm position, which in case of deep-inspiration or coughing may produce less accurate estimates of diaphragm position. Sudden deep inspirations do not occur during PBH and in our study none of the PBHs was prematurely stopped due to coughing, potentially resulting in more accurate tracking of the diaphragm during PBH.

The applicability of the RHT as surrogate for abdominal organ motion in tracking depends on the ability of the RHT to be tracked during radiation treatments. Hindley et al. have shown that real-time tracking of the right hemidiaphragm was feasible in six lung cancer patients during FB using kV imaging on a conventional linear accelerator. The diaphragm could be tracked successfully and lung tumor displacement could be estimated with localization errors of 1.6–6.7 mm, 1.2–4.0 mm, and 0.5–3.1 mm in the IS, AP and LR directions, respectively.[41] Potentially, these localization errors could be reduced when tracking would be performed during PBH. Alternatively, when tracking would not be feasible, diaphragm motion could be determined using cone-beam CT at the start of a treatment fraction. Subsequently, the intra-fractional organ motion can be derived using the DR to design an optimal adaptive plan.

5 | CONCLUSION

Displacements of abdominal organs highly correlate with displacements of the RHT during PBH. The error when using the RHT as surrogate for abdominal organ motion are at median between 0.13 and 0.31 cm for each centimeter of RHT displacement and between 0.4 and 0.8 mm per minute of breath-holding. Therefore, the RHT can serve as a surrogate for abdominal organ motion in radiotherapy, for example, during tracking, provided that the small estimation error is taken into account in the margins.

ACKNOWLEDGMENTS

We would like to thank our radiotherapy technicians Femke Beeksma, Myrte Boon and Katinka Tijman for supporting this study by operating the MR scanner and acquiring imaging data. JV is a PhD student supported by the Dutch Cancer Society (KWF, project number 12900). MP is supported by a Marie Skłodowska-Curie Individual Fellowship (number 894619).

CONFLICT OF INTEREST

Prof. dr. Bel is involved in several projects sponsored by Elekta and Varian, outside of this work. Elekta and Varian have no involvement in this study whatsoever.

DATA AVAILABILITY STATEMENT

The datasets generated and/or analyzed during the current study are not publicly available since the volunteers did not consent in sharing the data with third parties.

CONSENT FOR PUBLICATION

The figures depicting volunteer's data are unidentifiable and there are no details on volunteers reported within the manuscript. Therefore, separate consent for publication is not deemed necessary for the figures shown in this manuscript.

REFERENCES

1. Keall PJ, Mageras GS, Balter JM, et al. The management of respiratory motion in radiation oncology report of AAPM Task Group 76 a. *Med Phys*. 2006;33(10):3874-3900. doi:10.1118/1.2349696
2. Spindeldreier CK, Klüter S, Hoegen P, et al. MR-guided radiotherapy of moving targets. *Radiologe*. 2021;61(Suppl 1):39-48. doi:10.1007/S00117-020-00781-4

3. Remmerts de Vries IF, Dahele M, Mostafavi H, Slotman B, Verbakel W. Markerless 3D tumor tracking during single-fraction free-breathing 10MV flattening-filter-free stereotactic lung radiotherapy. *Radiother Oncol*. 2021;164:6-12. doi:10.1016/j.radonc.2021.08.025
4. Katoh N, Onimaru R, Sakuhara Y, et al. Real-time tumor-tracking radiotherapy for adrenal tumors. *Radiother Oncol*. 2008;87(3):418-424. doi:10.1016/J.RADONC.2008.03.013
5. Quirk S, Becker N, Smith WL. External respiratory motion analysis and statistics for patients and volunteers. *J Appl Clin Med Phys*. 2013;14(2):90-101. doi:10.1120/JACMP.V14I2.4051
6. Tran EH, Eiben B, Wetscherek A, et al. Evaluation of MRI-derived surrogate signals to model respiratory motion. *Biomed Phys Eng Express*. 2020;6:45015. doi:10.1088/2057-1976/ab944c
7. Siva S, Pham D, Gill S, et al. An analysis of respiratory induced kidney motion on four-dimensional computed tomography and its implications for stereotactic kidney radiotherapy. *Radiat Oncol*. 2013;8(1):1-8. doi:10.1186/1748-717X-8-248
8. Yang J, Cai J, Wang H, et al. Is diaphragm motion a good surrogate for liver tumor motion? *Int J Radiat Oncol Biol Phys*. 2014;90(4):952-958. doi:10.1016/J.IJROBP.2014.07.028
9. Feng M, Balter JM, Normolle D, et al. Characterization of pancreatic tumor motion using cine MRI: surrogates for tumor position should be used with caution. *Int J Radiat Oncol Biol Phys*. 2009;74(3):884-891. doi:10.1016/J.IJROBP.2009.02.003
10. Caines R, Sisson NK, Rowbottom CG. 4DCT and VMAT for lung patients with irregular breathing. *J Appl Clin Med Phys*. 2022;23(1). doi:10.1002/acm2.13453
11. Wikström KA, Isacsson UM, Pinto MC, Nilsson KM, Ahnesjö A. Evaluation of irregular breathing effects on internal target volume definition for lung cancer radiotherapy. *Med Phys*. 2021;48(5):2136-2144. doi:10.1002/mp.14824
12. Cai J, Chang Z, Jennifer O, et al. Investigation of sliced body volume (SBV) as respiratory surrogate. *J Appl Clin Med Phys*. 2013;14(1):71-80. doi:10.1120/JACMP.V14I1.3987
13. Park S, Farah R, Shea SM, Tryggestad E, Hales R, Lee J. Simultaneous tumor and surrogate motion tracking with dynamic MRI for radiation therapy planning. *Phys Med Biol*. 2018;63(2). doi:10.1088/1361-6560/aaa20b
14. Lens E, van der Horst A, Versteijne E, Bel A, van Tienhoven G. Considerable pancreatic tumor motion during breath-holding. *Acta Oncol (Madr)* 2016;55(11):1360-1368. doi:10.1080/0284186X.2016.1221532
15. Parkes MJ. Breath-holding and its breakpoint. *Exp Physiol*. Published online 2006:1-15. doi:10.1113/expphysiol.2005.031625
16. Parkes M, Cashmore J, Green S, et al. Defining short and prolonged breath-holds. *Br J Radiol*. 2020;93(1111). doi:10.1259/bjr.20200191
17. van Kesteren Z, Veldman JK, Parkes MJ, et al. Quantifying the reduction of respiratory motion by mechanical ventilation with MRI for radiotherapy. *Radiat Oncol*. 2022;17(1):1-11. doi:10.1186/S13014-022-02068-5
18. Barten DLJ, Laan JJ, Nelissen KJ, et al. A 3D cine-MRI acquisition technique and image analysis framework to quantify bowel motion demonstrated in gynecological cancer patients. *Med Phys*. 2021;48(6):3109-3119. doi:10.1002/MP.14851
19. Stemkens B, Tijssen RHN, De Senneville BD, et al. Optimizing 4-dimensional magnetic resonance imaging data sampling for respiratory motion analysis of pancreatic tumors. *Int J Radiat Oncol Biol Phys*. 2015;91(3):571-578. doi:10.1016/j.ijrobp.2014.10.050
20. Mazur TR, Fischer-Valuck BW, Wang Y, Yang D, Mutic S, Li HH. SIFT-based dense pixel tracking on 0.35 T cine-MR images acquired during image-guided radiation therapy with application to gating optimization. *Med Phys*. 2016;43(1):279-293. doi:10.1118/1.4938096
21. Preiswerk F, De Luca V, Arnold P, et al. Model-guided respiratory organ motion prediction of the liver from 2D ultrasound. *Med Image Anal*. 2014;18(5):740-751. doi:10.1016/j.media.2014.03.006
22. Parkes MJ, Green S, Stevens AM, Parveen S, Stephens R, Clutton-Brock TH. Safely prolonging single breath-holds to >5min in patients with cancer; feasibility and applications for radiotherapy. *Br J Radiol*. 2016;89(1063). doi:10.1259/BJR.20160194
23. Klein S, Staring M, Murphy K, Viergever MA, Pluim JPW. Elastix: a toolbox for intensity-based medical image registration. *IEEE Trans Med Imaging*. 2010;29(1):196-205. doi:10.1109/TMI.2009.2035616
24. Metz CT, Klein S, Schaap M, van Walsum T, Niessen WJ. Nonrigid registration of dynamic medical imaging data using nD + t B-splines and a groupwise optimization approach. *Med Image Anal*. 2011;15(2):238-249. doi:10.1016/J.MEDIA.2010.10.003
25. Christensen GE, Johnson HJ. Consistent image registration. *IEEE Trans Med Imaging*. 2001;20(7):568-582. doi:10.1109/42.932742
26. Riyahi S, Choi W, Liu C-J, et al. Quantifying local tumor morphological changes with Jacobian map for prediction of pathologic tumor response to chemo-radiotherapy in locally advanced esophageal. *Phys Med Biol*. 2018;63:145020. doi:10.1088/1361-6560/aacd22
27. Schmidt K-H, Jurado B, Bender ET, Tomé WA. The utilization of consistency metrics for error analysis in deformable image registration. *Phys Med Biol*. 2009;54:5561-5577. doi:10.1088/0031-9155/54/18/014
28. Vanderburg A, Latham DW, Buchhave LA, et al. Deformation field validation and inversion applied to adaptive radiation therapy. *Phys Med Biol*. 2013;58(15):5269. doi:10.1088/0031-9155/58/15/5269
29. Fedorov A, Beichel R, Kalpathy-Cramer J, et al. 3D Slicer as an image computing platform for the Quantitative Imaging Network. *Magn Reson Imaging*. 2012;30(9):1323-1341. doi:10.1016/J.MRI.2012.05.001
30. Brix L, Ringgaard S, Sangild Sørensen T, Rugaard Poulsen P. Three-dimensional liver motion tracking using real-time two-dimensional MRI. *Med Phys*. 2014;41(4):04302-1-04302-10. doi:10.1118/1.4867859
31. Rohlfing T, Maurer Jr C. Modeling liver motion and deformation during the respiratory cycle using intensity-based nonrigid registration of gated MR images. *Med Phys*. 2004;31(3):427-432. doi:10.1118/1.1644513
32. Von Siebenthal M, Székely G, Lomax AJ, Cattin PC. Systematic errors in respiratory gating due to intrafraction deformations of the liver. *Med Phys*. 2007;34(9):3620-3629. doi:10.1118/1.2767053
33. Nason LK, Walker CM, Mcneeley MF, Burivong W, Fligner CL, David Godwin J. Imaging of the diaphragm: anatomy and function. *Radiographics*. 2012;32(2). doi:10.1148/RG.322115127
34. Bleeker M, Hulshof MCCM, Bel A, Sonke JJ, van der Horst A. Gastric deformation models for adaptive radiotherapy: personalized vs population-based strategy. *Radiother Oncol*. 2022;166:126-132. doi:10.1016/J.RADONC.2021.11.028
35. Huijskens SC, Van Dijk IWEM, Visser J, et al. Abdominal organ position variation in children during image-guided radiotherapy. *Radiat Oncol*. 2018;13(1):1-9. doi:10.1186/S13014-018-1108-9
36. Mao W, Kim J, Chetty IJ. Association between internal organ/liver tumor and external surface motion from cine MR images on an MRI-linac. *Front Oncol*. 2022;12. doi:10.3389/FONC.2022.868076
37. Kim TG, Kang KM, Park B, et al. Interfractional diaphragmatic position variation according to stomach volume change during respiratory-gated radiotherapy for hepatocellular carcinoma. *Med Phys*. 2021;48(9):5531-5539. doi:10.1002/MP.15055
38. Langen KM, Jones DTL. Organ motion and its management. *Int J Radiat Oncol Biol Phys*. 2001;50(1):265-278. doi:10.1016/S0360-3016(01)01453-5

39. Lens E, Gurney-Champion OJ, Tekelenburg DR, et al. Abdominal organ motion during inhalation and exhalation breath-holds: pancreatic motion at different lung volumes compared. *Radiother Oncol*. 2016;121(2):268-275. doi:10.1016/j.radonc.2016.09.012
40. Parkes MJ, Green S, Kilby W, Cashmore J, Ghafoor Q, Clutton-Brock TH. The feasibility, safety and optimization of multiple prolonged breath-holds for radiotherapy. *Radiother Oncol*. 2019;141:296-303. doi:10.1016/j.radonc.2019.06.014
41. Hindley N, Keall P, Booth J, Shieh CC. Real-time direct diaphragm tracking using kV imaging on a standard linear accelerator. *Med Phys*. 2019;46(10):4481-4489. doi:10.1002/MP.13738

SUPPORTING INFORMATION

Additional supporting information can be found online in the Supporting Information section at the end of this article.

How to cite this article: Veldman JK, van Kesteren Z, Gunwhy ER, et al. Accuracy of abdominal organ motion estimation in radiotherapy using the right hemidiaphragm top as a surrogate during prolonged breath-holds quantified with MRI. *Med Phys*. 2023;1-12. https://doi.org/10.1002/mp.16403